Journal of Statistical Mechanics: Theory and Experiment
An IOP and SISSA journal

The unstructured lattice Boltzmann method for non-Newtonian flows

G Pontrelli[1], **S Ubertini**[2] **and S Succi**[1]

[1] IAC-CNR, Via dei Taurini 19, 00185 Roma, Italy
[2] Department of Technology, University 'Parthenope', Napoli, Italy
E-mail: g.pontrelli@iac.cnr.it, stefano.ubertini@uniparthenope.it and s.succi@iac.cnr.it

Received 29 October 2008
Accepted 14 December 2008
Published 10 June 2009

Online at stacks.iop.org/JSTAT/2009/P06005
doi:10.1088/1742-5468/2009/06/P06005

Abstract. Non-Newtonian models with shear-thinning viscosity are commonly used to solve a variety of complex flow problems. A new finite-volume discretization based upon an unstructured grid is used to integrate the differential form of the lattice Boltzmann equation with a shear-dependent viscosity, using a cell-vertex finite-volume technique. The unknown fields are placed at the nodes of the mesh and evolve on the basis of the fluxes crossing the surfaces of the corresponding control volumes. Numerical results show a satisfactory accuracy also in the case of relatively complex geometries and demonstrate the ability of the method to predict the main features of non-Newtonian flows in straight and stenosed channels.

Keywords: hydrodynamics of complex fluids and biological fluid dynamics, lattice Boltzmann methods, computational fluid dynamics

J. Stat. Mech. (2009) P06005

Contents

1. Introduction

In the last decade LB methods have undergone major progress as an alternative to the discretization of the Navier–Stokes equations for the numerical solution of complex fluid problems [1]. The LB method is based on a minimal kinetic Boltzmann equation in which representative particles evolve on a regular Cartesian grid according to simple streaming and collision rules, designed in such a way as to preserve the basic symmetries (conservation laws) of fluid dynamics. The LBM exhibits a number of appealing features as a computational fluid dynamic solver, such as the simplicity of the stream-and-collide dynamics, its amenability to parallel computing and its ease of use in handling complex flows. Another key property of LB, with respect to Navier–Stokes equations, is that non-linearities are local (quadratic dependence of the local equilibrium on the flow field) and the non-localities are linear, because advection proceeds along constant, straight lines defined by the discrete speeds. In particular, owing to its kinetic nature, the pressure field and the stress tensor are locally available, with no need for solving any (expensive) Poisson problem. This is particularly important for modeling non-Newtonian fluids which exhibit a non-linear response to stress and are usually modeled through a viscosity that changes with the applied shear rate. However, the original LB method has to be designed on a uniform Cartesian grid. This represents a severe limitation for practical engineering purposes, especially for flows in complex geometries and/or for high resolutions near the body or the walls [2]. Among the recent advances that have led to substantial enhancement of the capabilities of the method for handling irregular shapes [3, 4], a particularly interesting option is represented by finite-volume

doi:10.1088/1742-5468/2009/06/P06005

J. Stat. Mech. (2009) P06005

formulations on fully unstructured grids (unstructured lattice Boltzmann schemes or ULBE for short) [5, 6]. To date, ULBE implementations were limited to Newtonian fluids simulations. However, in some applications, such as those involving physiological flows, the fluid cannot be treated as Newtonian, and a more realistic rheological models should be used [7]–[9]. In this paper we present the first extension of ULBE to non-Newtonian fluids, with an application to hemodynamic flows. The use of ULBE for blood flow simulations combines the advantages of the LBM for non-Newtonian fluids to the enhanced geometrical flexibility, as the use of an unstructured grid allows one to accommodate the complex geometries typical of blood vessels (bifurcation, branching, and curvatures) with a limited number of nodes. Moreover, as in ULBE the body surface is defined by grid points (while in standard LBM the body surface does not generally lie on lattice sites), both pressure and viscous forces are locally available at the walls and explicitly expressed in terms of the distribution function, thus making the wall shear stress calculation straightforward. This is important in hemodynamics, where an accurate knowledge of the wall shear stress is highly valued.

As a starting point, because of the complexity of the constitutive equation, only a steady state case is considered in this paper. A constant flow rate is imposed and the wall deformability is disregarded. The mathematical model is the shear-thinning Carreau model, able to describe steady flows for the typical range of shear rates [9, 10]. As a fundamental study, a couple of basic flow configurations are considered: an excellent agreement with the literature data for a straight pipe is obtained and the typical flow fields in constricted tubes are well reproduced.

2. The unstructured lattice Boltzmann equation

The LB method can be regarded as a mesoscopic (between microscopic and macroscopic) approach for modeling macroscopic hydrodynamics. Rather than following the position and velocity of each particle in the system, as is done in microscopic models (i.e. molecular dynamics), the fluid flow is described by tracking the evolution of the density distribution function (or population) $f_i(\vec{x}, t) \equiv f(\vec{x}, \vec{v} = \vec{c}_i, t)$, $i = 1, b$ that describes the probability of finding a particle at site $\vec{x}$, at time t moving along the lattice direction defined by the discrete speed $\vec{c}_i$. The time rate of change of the particle distribution function is given by the following discrete Boltzmann equation:

$$\partial_t f_i + \vec{c}_i \cdot \vec{\nabla} f_i = -(f_i - f_i^{\mathrm{eq}})/\tau \tag{1}$$

in which the left-hand side represents the molecular free streaming, whereas the right-hand side represents molecular collisions via a single-time relaxation towards local equilibrium f_i^{eq} on a typical timescale τ [4]. The latter is called the relaxation time or relaxation parameter and, in macroscopic terms, it defines the fluid viscosity.

The local equilibrium is given by the expansion in Taylor series of the Maxwell–Boltzmann distribution:

$$f_i^{\mathrm{eq}} = \rho w_i \left[1 + \beta u_i + \frac{\beta^2}{2}(u_i^2 - u^2)\right] \tag{2}$$

where $\beta = 1/c_{\mathrm{s}}^2$, c_{s} being the lattice sound speed, ρ the fluid density, $\vec{u}$ the fluid speed, $u_i \equiv \vec{u} \cdot \vec{c}_i$ and w_i are the associated weight coefficients.

J. Stat. Mech. (2009) P06005

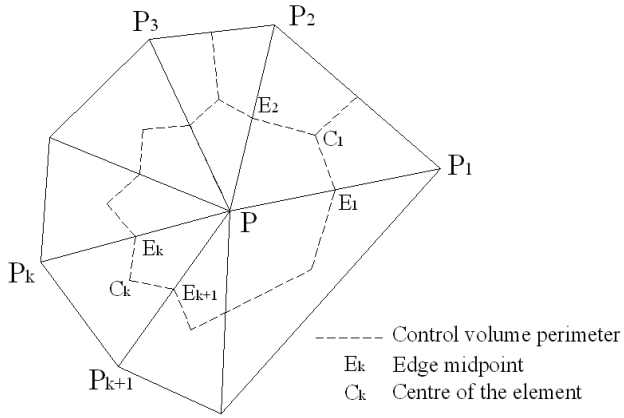

Figure 1. Geometrical layout of the cell-vertex finite-volume discretization around a grid point P.

One of the key properties of the LB method is that only a very limited set of discrete speeds $\vec{c}_i$ needs to be retained for hydrodynamic purposes, so that LB is orders of magnitudes less expensive than microscopic simulation methods.

In order to recover the correct fluid dynamic equations in the macroscopic limit, the set of discrete speeds must satisfy mass, momentum and energy conservation, as well as rotational symmetry. It should be noted that only a limited class of lattices exhibits the right symmetry to ensure the conservation constraints. In the present work we shall refer to the two-dimensional nine-speed model (known as D2Q9) with given discrete speeds $\vec{c}_i$ and weights w_i [6]. In the limit of weak departures from local equilibrium (i.e. small Knudsen numbers), it has been demonstrated that the above formulation recovers the dynamic behavior of a fluid with kinematic viscosity $\nu = c_s^2\tau$ [6]. The macroscopic local quantities may be computed at any instant during the evolution by taking the appropriate discrete velocity moments of the distribution functions: $\rho = \sum_i f_i$ and $\vec{u} = \sum_i \vec{c}_i f_i/\rho$. The fluid pressure is given by $P = \rho c_s^2$.

The ULBE approach for numerically solving equation (1) is a finite-volume scheme of the cell-vertex type, using a tessellation based on triangular elements. The use of unstructured grids with control volumes of arbitrary triangular shape allows local and *heterogeneous* forms of grid refinements which are beyond reach of the standard BGK. However, the time-stepping procedure suffers from stricter stability constraints. The nine discrete populations $f_i(\vec{x}, t)$ associated with each node P of the discrete grid (figure 1) represent the unknowns of the problem. The finite volume over which equation (1) is integrated is defined by means of the set of K triangles, which share P as a common vertex. Since the discrete grid is unstructured, each node is identified by its coordinates and the connectivity (P, P_k, P_{k+1} in figure 1) is free to change from node to node. As shown in figure 1, the portion of the control volume [$C_k, E_k, P, E_k + 1$] that refers to the kth triangular element is built through the union of the two sub-grid triangles $\Omega_k^- = [P, E_k, C_k]$ and $\Omega_k^+ = [P, C_k, E_{k+1}]$, where C_k is the center of the grid element and E_k and $E_k + 1$ are the mid-points of the edges that share P as a common vertex. Populations at off-grid points E_k and C_k are calculated with standard linear interpolations. Application of the Gauss theorem to each finite-volume portion yields the following set of ordinary

J. Stat. Mech. (2009) P06005

differential equations:

$$\frac{\mathrm{d}f_i(P,t)}{\mathrm{d}t} = \frac{1}{V_P}\sum_k (\Phi_{ik} - \Xi_{ik}) \tag{3}$$

where the sum $k = 0, K$ runs over the control volume $\Omega_P = \cup_k \Omega_k$ obtained by joining the centers C_k with edge mid-points E_k, V_P is the control volume associated with P and the index $k = 0$ denotes the pivotal point P. Φ_{ik} indicate the fluxes associated with the streaming operator and Ξ_{ik} the integral of the collision operator of the ith population at the kth node, respectively. The ULBE takes the following general form:

$$\frac{\mathrm{d}f_i(P,t)}{\mathrm{d}t} = \sum_{k=0}^{K} S_{ik} f_i(P_k,t) - \sum_{k=0}^{K} \frac{C_{ik}[f_i(P_k,t) - f_i^{\mathrm{eq}}(P_k,t)]}{\tau} \tag{4}$$

where the detailed expressions for the streaming and collision matrices S_{ik} and $C_{ik} = C_k\delta_{ik}$ can be found in [6]. By definition the following sum rules apply:

$$\sum_{k=0}^{K} S_{ik} = 0, \qquad \sum_{k=0}^{K} C_{ik} = 1, \quad \forall i.$$

In [6] it was shown that the ULBE scheme recovers hydrodynamics with the same viscosity of the continuum, $\nu = c_{\mathrm{s}}^2\tau$, and that numerical viscosity effects are within second order of accuracy in space. It is important to highlight that with a forward Euler time marching scheme the maximum time step allowed by the numerical stability condition is

$$\Delta t < 2\tau \tag{5}$$

[11].

This condition, combined with the expression for the fluid viscosity $\nu = c_s^2\tau$, indicates that small viscosities can only be attained by making the time step correspondingly small.

2.1. Boundary conditions

An important feature of the ULBE method is that boundary conditions are incorporated in a straightforward way by means of the so-called *covolume method* [5]. Any boundary condition for ULBE needs to cope with the fact that the corresponding control volumes do not close up, leaving two external edges exposed on the boundary. With the covolume method, the boundary nodes are treated exactly as fluid nodes with the only difference being that the edge fluxes are evaluated explicitly by using interpolation at the boundary edges, thus taking part in the matrix S_{ik} definition. The boundary condition is then given in terms of enforced macroscopic values in the equilibrium distribution function (i.e. $u = 0$ for the no-slip boundary condition). The covolume works for the generic boundary geometries and has proven to support relatively strong boundary gradients. At least one regular buffer at inlet/outlet sections is necessary for open flows when a null or constant velocity/pressure gradient is given as a boundary condition. The use of multiple buffers is beneficial to the stability of ULBE computations for open flows. For more details on boundary conditions refer to [12].

doi:10.1088/1742-5468/2009/06/P06005

J. Stat. Mech. (2009) P06005

3. Extension of ULBE to non-Newtonian models

We shall now generalize the ULBE scheme to the case non-Newtonian (NN) flows, where a shear-rate-dependent viscosity law $\mu(\dot\gamma)$ is imposed. To this end, the constant time relaxation τ in equations (1) and (4) is replaced by a self-consistent, shear-dependent $\tau(\dot\gamma)$, $\dot\gamma = \dot\gamma[f_i]$ being the shear rate, a function(al) of the density distribution function f. The current value $\dot\gamma$ is obtained by the following considerations. In LBM, the strain and stress tensors $\mathbf{\Gamma}$ and $\mathbf{\Pi}$ can be written explicitly in terms of the particle distribution functions, respectively as [8, 13]

$$\mathbf{\Gamma}_{\alpha\beta} = -\frac{1}{2\rho\tau c_s^2}\mathbf{\Pi}_{\alpha\beta} \tag{6}$$

where

$$\mathbf{\Pi}_{\alpha\beta} = \sum_i (f_i - f_i^{\mathrm{eq}})\boldsymbol{c}_{i\alpha}\boldsymbol{c}_{i\beta} \tag{7}$$

and α, β run over spatial dimensions. Let us now introduce a measure of the magnitude of the previous tensors (norm):

$$\dot\gamma \equiv 2|\mathbf{\Gamma}| = 2\sqrt{\sum_{\alpha,\beta}\Gamma_{\alpha\beta}\Gamma_{\alpha\beta}}, \qquad \sigma \equiv |\mathbf{\Pi}| = \sqrt{\sum_{\alpha,\beta}\Pi_{\alpha\beta}\Pi_{\alpha\beta}}. \tag{8}$$

The strain–stress relationship (6) can be rewritten (*averaged*) as

$$\dot\gamma = \frac{\sigma}{\rho\tau(\dot\gamma)c_s^2} \tag{9}$$

and, as $\mu(\dot\gamma) = \rho\nu(\dot\gamma) = \rho c_s^2\tau(\dot\gamma)$, we have

$$\sigma = \mu(\dot\gamma)\dot\gamma. \tag{10}$$

In principle $\dot\gamma$ must be obtained by solving the above non-linear equation (10) by iteration at each lattice site. However, due to the slow variation of $\mu(\dot\gamma)\dot\gamma$ on a timescale Δt, current practice shows that one can adjust τ along the time integration as follows:

$$\tau(t+\Delta t) = \frac{\mu\left[\dot\gamma(t), t\right]}{\rho(t)c_s^2}. \tag{11}$$

Note that equation (10) yields the standard scalar relation $\sigma = \mu\dot\gamma$ in the Newtonian case.

3.1. Statistical mechanics of ULBE and multiscale applications

The set of ULBE equation (4) can be mapped onto a *mesoscopic* discrete dynamical system, living in an irregular spacetime defined by the set of N lattice nodes P_k and their connectivity. In abstract notation,

$$\frac{\mathrm{d}f}{\mathrm{d}t} = (S - \tau^{-1}C)f + \tau^{-1}C\ f^{\mathrm{eq}} \tag{12}$$

where $f(t)$ represents an N-dimensional state vector and S and C stand for the streaming and collision operators, i.e. sparse matrices whose structure is fixed by the lattice connectivity. For the case of NN flows, this system is also *adaptive*, in that the dynamics

J. Stat. Mech. (2009) P06005

of the state vector $f(t) \equiv f(P_k, t)$, $k = 1, \ldots, N$, is coupled to the self-consistent dynamics of the relaxation parameter τ via the local, dynamic constitutive relations equations (9) and (10). Note that within the mesoscopic ULBE representation, the parameter τ fixes the typical time of return to local equilibrium, or, alternatively, the lifetime of non-equilibrium excitations. In a Newtonian fluid, this timescale is everywhere the same, which means that when moving from one node to another, the populations not only have to readjust to a different local equilibrium (due to the inhomogeneity of the flow fields), but also their readjustment time is differs from place to place, depending on the local strain conditions. In particular, for the case of blood flows, higher strains are associated with shorter relaxation time. This clearly adds to the complexity of the dynamic behavior of the system. We note that a similar mechanism applies to the case of turbulent flows, albeit in the opposite direction: high strains are associated with larger effective viscosities, and hence longer relaxation time [14].

The ULBE-like equations may represent a paradigm for the mesoscopic representation of a broad class of complex flowing systems, possibly extending beyond the specific realm of hydrodynamics. As a result, the systematic analysis of the statistical mechanics (kinetic theory) of ULBE-like systems with self-consistent/adaptive relaxation dynamics may constitute an interesting topic for future research in statistical mechanics. Finally, since ULBE permits one to place degrees of freedom where actually needed, important applications can also be envisaged for future multiscale applications, whereby ULBE would be used in selected subregions of the flow, typically near walls, and coupled to more microscopic models, such as molecular dynamics.

4. Validation of the Newtonian and power-law models

As first test problem, let us consider a basic 2D steady flow between parallel plates located at $\pm H$ and driven by a constant pressure gradient G. In the case of constant viscosity μ_0 (Newtonian fluid) and for a fully developed flow, this is the plane Poiseuille flow that constitutes the basis for testing more complex flow regimes. For a fully developed flow, the exact solution is

$$u_N(y) = \frac{G}{2\mu_0}\left(H^2 - y^2\right) = U_{\max}\left(1 - \frac{y^2}{H^2}\right). \tag{13}$$

Also for the power-law model $\mu(\dot{\gamma}) = m|\dot{\gamma}|^{n-1}$, with $0 < n < 1$, an exact solution is available:

$$u_{\mathrm{PL}}(y) = \left(\frac{G}{m}\right)^{1/n}\left(\frac{n}{n+1}\right)H^{(n+1)/n}\left(1 - \left(\frac{|y|}{H}\right)^{(n+1)/n}\right) = U_{\max}\left[1 - \left(\frac{|y|}{H}\right)^{(n+1)/n}\right]. \tag{14}$$

To check the accuracy and robustness of ULBE, we compare the numerical result of Newtonian and power-law model with the above analytical solutions (13) and (14).

Note that in the power-law model the viscosity may attain extremely large or excessively small values. For example, in a shear-thinning fluid $\mu \to 0$ when $\dot{\gamma} \to \infty$ and, consequently, $\tau \to 0$. To avoid such limiting (and unrealistic) cases, the higher or

J. Stat. Mech. (2009) P06005

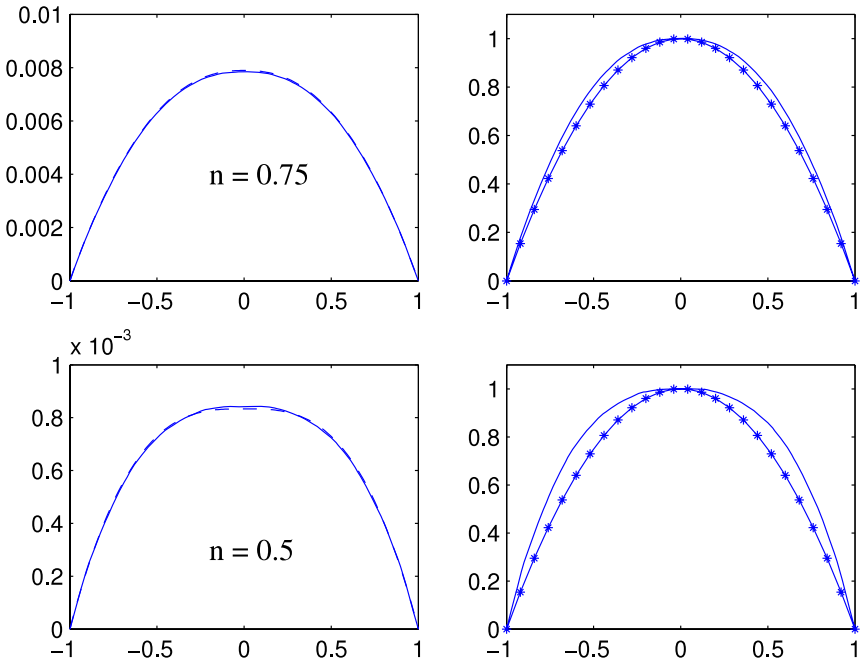

Figure 2. Velocity profiles for power-law model $G = 5 \times 10^{-5}, \mu_{\max} = 0.1, \mu_{\min} = 0.001$ (see equation (15)), $\Delta t = 0.01$. On the left, the comparison with the analytical solution (equation (14); dashed line); on the right, that with the normalized Newtonian solution ($n = 1$, equation (13); starred line, LB units).

lower viscosities over a given threshold are cut off through the following law:

$$\mu(\dot\gamma) = \begin{cases} m\dot\gamma_0^{n-1} = \mu_{\max} & \text{if } \dot\gamma < \dot\gamma_0 \\ m\dot\gamma^{n-1} & \text{if } \dot\gamma_0 < \dot\gamma < \dot\gamma_\infty \\ m\dot\gamma_\infty^{n-1} = \mu_{\min} & \text{if } \dot\gamma > \dot\gamma_\infty \end{cases} \tag{15}$$

(see [15]). The case with $G = 5 \times 10^{-5}, m = 10^{-3}$ has been simulated with $n = 0.5$ and 0.75. The viscosity has been truncated according to $\mu_{\min} = 0.001$ (never reached in the simulations) and $\mu_{\max} = 0.1$. Figure 2 show an excellent matching with the power-law analytical solution (left) and the difference from the Newtonian case ($n = 1$; right).

5. Simulation of steady flows

To simulate a physiological case, we consider a shear-dependent viscosity that follows the Carreau model:

$$\mu(\dot\gamma) = \mu_\infty + (\mu_0 - \mu_\infty)\left(1 + (\lambda\dot\gamma)^2\right)^{(n-1)/2} \tag{16}$$

with the following rheological parameters [10, 16]:

$$\mu_0 = 0.56P \qquad \mu_\infty = 0.0345P \qquad \lambda = 3.313s \qquad n = 0.3568. \tag{17}$$

To emphasize the NN shear-thinning effects, let us consider physical variables pertaining to smaller vessels (arterioles):

$$U_{\max} = 2 \text{ cm s}^{-1} \qquad H = 5 \times 10^{-3} \text{ cm} \qquad \rho = 1 \text{ g cm}^{-3}$$

J. Stat. Mech. (2009) P06005

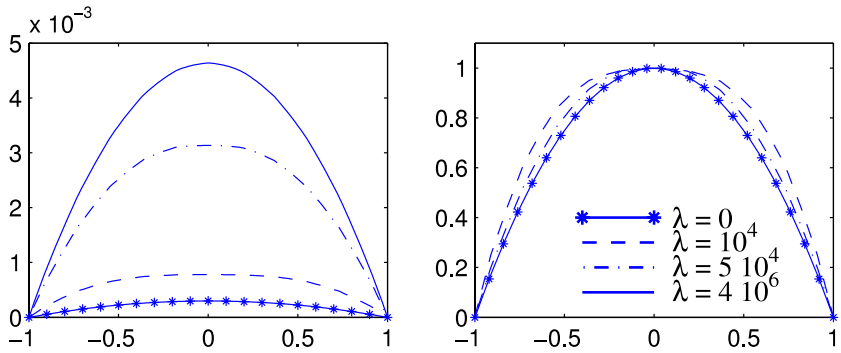

Figure 3. Velocity profiles (normalized on the right) in the case of the Carreau model $G = 10^{-5}$, with different λ s. Comparison with the Newtonian solution (starred line; LB units).

giving rise to a rather small Reynolds number:

$$\mathrm{Re}_0 = \frac{\rho U_{\max} H}{\mu_0} \approx 0.017.$$

The model has been tested against two typical idealized flow problems, such as those in a straight and through a contracted tube, driven by a constant pressure gradient.

5.1. Flow in a straight channel

In the LB simulations, let us consider a channel of semiwidth $\bar{H}$ where a fluid of density $\bar{\rho}$ and viscosity $\bar{\mu}$ is flowing under a constant forcing $\bar{G}$. To guarantee a mesoscopic flow regime comparable with the above physical values, a careful scaling between macroscopic and mesoscopic variables is carried out. A channel of length 10 has been covered by 4460 triangular cells, constituting a uniform grid with 2351 equally distributed nodes. The time step has been fixed initially as $\Delta t = 0.01$, and possibly reduced (halved) in order to guarantee that condition (5) is verified. As LB variables, we set

$$\bar{H} = 1 \qquad \bar{\rho} = 1 \qquad \bar{G} = 10^{-5}.$$

In the following, the overbar denoting LB variables is omitted. We have the following relationship in LB variables: $\Delta\rho = \Delta p/c_s^2 = G\,L/c_s^2$.

In figure 3 the velocity profiles corresponding to four time constants λ are displayed. The peak value of the velocity rises dramatically with λ, passing from a Newtonian regime with higher viscosity μ_0 to another Newtonian regime with a lower μ_∞. In the transition shear-thinning region, the parabolic shape appears flattened in the center of the channel. It turns out that λ plays a critical role, since its value affects the viscosity decay as well as the maximum shear rate.

5.2. Flow through a contraction

Let us consider a channel with the shape of a long rectangle except in a small region centered at $x = 0$ with a smooth contraction as described by the following regular function:

$$\frac{H(x)}{H_0} = 1 - \delta \mathrm{e}^{-\phi x^2} \tag{18}$$

J. Stat. Mech. (2009) P06005

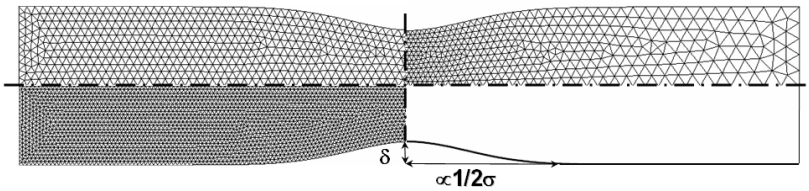

Figure 4. The axisymmetric stenosed rectangular channel defined by equation (15) covered by three grids: (a) uniform high resolution (left bottom), (b) uniform low resolution (left top), (c) non-uniform lower resolution (right top). The latter exhibits optimal properties in terms of accuracy and computational cost.

Table 1. Relative errors of v and τ on different grids.

	u	τ
E_{a-b}	0.096	0.057
E_{a-c}	0.076	0.041

where $H(x)$ is the height, $0 \leq \delta < 1$ is a measure of the degree of contraction, ϕ of its length (figure 4). The value of ϕ should be taken quite small to guarantee a slowly varying boundary profile. As a particular case, the rectangular channel is recovered for $\delta = 0$. The numerical parameters for the simulation are

$$H_0 = 5 \times 10^{-3} \text{ cm} \qquad \phi = 0.8 \qquad \delta = 0.3$$

corresponding to a degree of contraction of about 50% [17]. The pressure gradient, the rheological parameters and the LB settings are as in the straight channel flow.

5.2.1. Grid analysis. A sensitivity analysis on the grid size has been carried out. To this end, three different grid meshes have been selected—(a) uniform, high resolution (8569 nodes, reference case), (b) uniform, low resolution, (2205 nodes), (c) non-uniform, lower resolution (1737 nodes) refined in the contraction area. The three set of results have been compared. In particular, the relative difference of the horizontal velocity (u) across the throat and wall shear stress (τ) along the contraction segment have been considered by taking $E_{a-b}[x] = \sqrt{\sum (x_a - x_b)^2 / \sum x_a^2}$ as a measure of the relative error.

Table 1 shows that grid (c), in spite of the reduced number (−20%) of nodes with respect to grid (b), provides a better accuracy. This demonstrates the ULBE capability of clustering the degrees of freedom in the critical regions of the flow, without suffering any loss of accuracy, but actually enhancing it instead. These results confirm the grid analysis already performed for Newtonian flow simulations [12]. In the following simulations, the non-uniform mesh (c) has been chosen (figure 4). In the present NN model the limiting values for LB viscosities are $\mu_0 = 16.7 \times 10^{-3}$, $\mu_\infty = 1.03 \times 10^{-3}$, but the local viscosity in all simulations remains above the lower bound $\mu_{\min} = 2.011 \times 10^{-3}$. Figure 5 shows a typical complex pattern of viscosity, related to the strain distribution (see equation (16)).

J. Stat. Mech. (2009) P06005

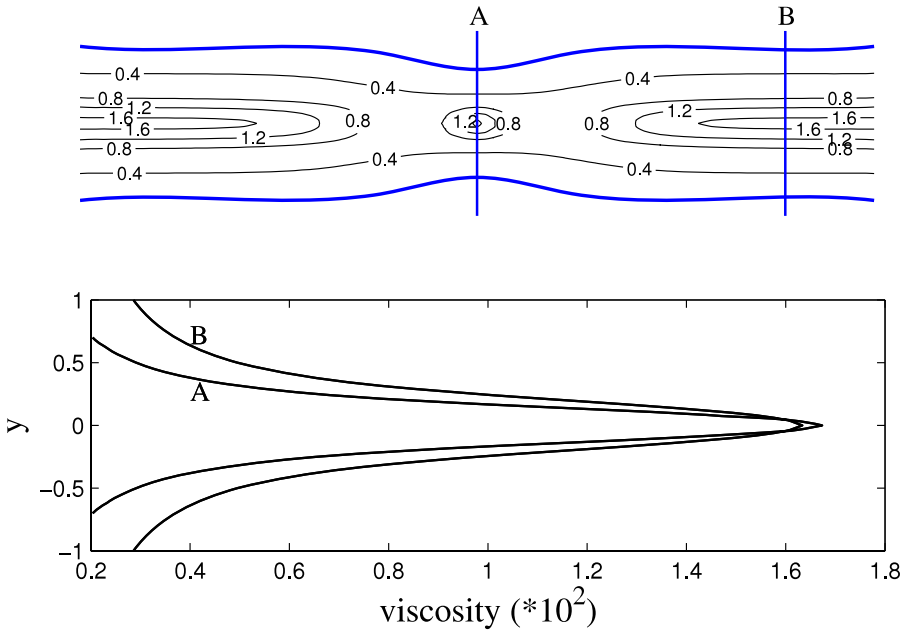

Figure 5. Viscosity contour lines (top) and profiles across sections A and B (bottom) for the Carreau model equation (16) ($G = 10^{-5}$, viscosity in LB units $\times\ 10^2$).

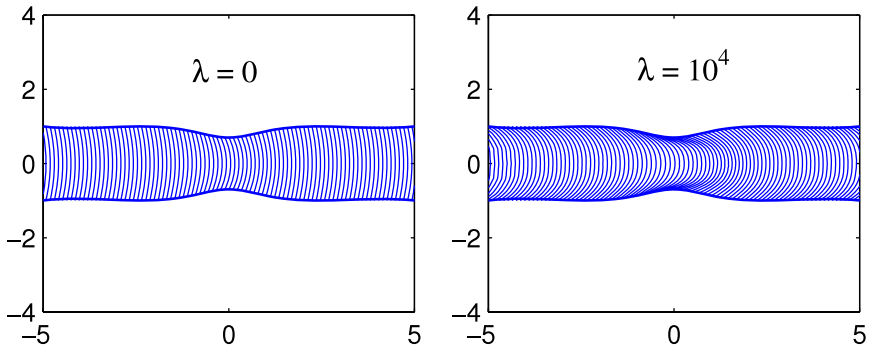

Figure 6. Velocity profiles across the stenosed channel in N (left) and NN cases (right). ($G = 10^{-5}$; LB units.)

5.2.2. Flow velocities. The velocity profiles are of some interest, since they provide a detailed description of the flow field. At that low Reynolds number and for such a mild contraction, no recirculation or flow reversal is present and the flow is symmetric upstream and downstream of the stenosis. The magnitude of velocity is much larger in the NN case (figure 6).

5.2.3. Pressure losses and wall shear stress. In the presence of a narrowing, the flow exhibits a resistance and hence an enhanced shear stress (i.e. the wall vorticity) and a pressure drop [18]. These are indicators of flow disturbances and are quantities of physiological relevance. Since there is no reliable method of determining the wall shear

J. Stat. Mech. (2009) P06005

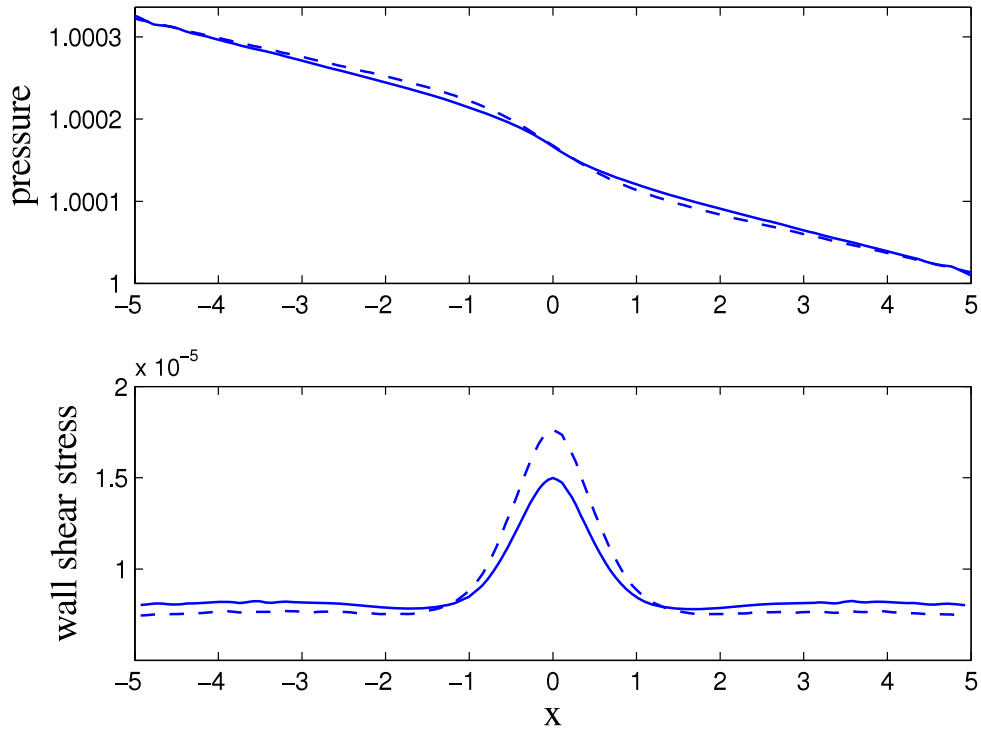

Figure 7. Pressure drop along the centerline (above) and wall shear stress (below) in a contracted channel ($G = 10^{-5}$, LB units). The difference between N ($\lambda = 0$, dashed line) and NN ($\lambda = 10^4$, continuous line) cases.

stress experimentally near the regions of possible reversal flow, the numerical experiments provide a very valuable (*non-invasive*) tool, because they offer a sufficiently accurate approximation of the flow configuration.

A pressure drop is observed as the occlusion is approached (figure 7). The wall shear stress (WSS) increases smoothly in correspondence with the contraction and has a peak value placed symmetrically at the center of the throat. Downstream, it goes back to the previous value. In the straight portion the WSS is higher in the NN case, and the opposite in the contraction, because of the lowered viscosity. In figure 5 the viscosity contour lines for NN case are shown. All these results are in qualitative agreement with those from other models existing in literature [19].

6. Conclusions

We have presented the first extension of the lattice Boltzmann method on unstructured grids to the case of non-Newtonian flows. The method has been validated for the case of hemodynamic flows in two-dimensional channels with straight walls and with constrictions. Despite their preliminary nature, these tests clearly demonstrate the ability of the ULBE method to gain accuracy by clustering the lattice nodes in the critical regions of the flow. Besides enhancing the accuracy of the hemodynamic simulations, this property may also prove very beneficial for future multiscale applications, coupling macroscopic hemodynamics with nanoparticle transport within the blood flow [20].

J. Stat. Mech. (2009) P06005

A thorough assessment of ULBE versus state of the art hemodynamic solvers, including standard LB, will require substantial benchmarking and quantitative comparison with the existing literature. Extension to three-dimensional flows in complex geometries, such as human arteries, stands out as a major topic for future research. Work along this direction is currently in progress.

Acknowledgments

This work has been partially supported by a bilateral CNR (Italy)–FCT (Portugal) grant: *Multiscale analysis and numerical simulation of mathematical models in hemodynamics and hemorheology*, 2007–2008.

References

[1] Benzi R, Succi S and Vergassola M, *The lattice Boltzmann equation: theory and applications*, 1992 *Phys. Rep.* **222** 145
[2] Buick J M, Cosgrove J A, Tonge S J, Mulholland A J, Steves B A and Collins M W, *The lattice Boltzmann equation for modelling arterial flows: reviews and applications*, 2003 *Int. Med.* **11** 1
[3] Cao N, Chen S, Jin S and Martinez D, *Physical symmetry and lattice symmetry in the lattice Boltzmann method*, 1997 *Phys. Rev.* E **55** R21
[4] Qian Y, d'Humieres D and Lallemand P, *Lattice BGK models for Navier–Stokes equation*, 1992 *Europhys. Lett.* **17** 479
[5] Peng G, Xi H and Duncan C, *Lattice Boltzmann method on irregular meshes*, 1998 *Phys. Rev.* E **58** R4124
[6] Ubertini S, Bella G and Succi S, *Unstructured lattice Boltzmann method: further developments*, 2002 *Phys. Rev.* E **68** 016701
[7] Malaspinas O, Courbebaisse G and Deville M, *Simulation of generalized Newtonian fluids with the lattice Boltzmann method*, 2007 *Int. J. Mod. Phys.* C **18** 1939
[8] Ouared R and Chopard B, *Lattice Boltzmann simulations of blood flow: non-Newtonian rheology and clotting processes*, 2005 *J. Stat. Phys.* **101** 209
[9] Artoli A M and Sequeira A, *Mesoscopic simulations of unsteady shear-thinning flows*, 2006 *Lect. Notes Comput. Sci.* **3992** 78
[10] Boyd J, Buick J M and Green S, *Analysis of the Casson and Carreau–Yasuda non-Newtonian blood models in steady and oscillatory flow using the lattice Boltzmann method*, 2007 *Phys. Fluids* **19** 093103
[11] Ubertini S and Succi S, *A generalised lattice Boltzmann equation on unstructured grids*, 2008 *Commun. Comput. Phys.* **3** 342
[12] Ubertini S and Succi S, *Recent advances of lattice Boltzmann techniques on unstructured grids*, 2005 *Prog. Comput. Fluid Dyn.* **5** 84
[13] Chopard B, Ouared R and Rufenacht D A, *A lattice Boltzmann simulation of clotting in stented aneurysms and comparison with velocity or shear rate reductions*, 2006 *Math. Comput. Simul.* **72** 108
[14] Chen H *et al*, *Extended Boltzmann kinetic equation for turbulent flows*, 2003 *Science* **301** 633
[15] Gabbanelli S, Drazer G and Koplik J, *Lattice-Boltzmann method for non-Newtonian (power-law) fluids*, 2005 *Phys. Rev.* E **72** 046312
[16] Artoli A M, Janela J and Sequeira A, *The role of Womersley number in shear-thinning fluids*, 2006 *WSEAS Trans. Fluid Mech.* **1** 133
[17] Pontrelli G, *Blood flow through an axisymmetric stenosis*, 2001 *Proc. Inst. Mech. Eng.* H **215** 1
[18] Lee K W and Xu X Y, *Modelling of flow and wall behaviour in a mildly stenosed tube*, 2002 *Med. Eng. Phys.* 575
[19] Jung H, Choi J W and Park C G, *Asymmetric flows of non-Newtonian fluids in symmetric stenosed artery*, 2004 *Korea–Australia Rheol. J.* 101
[20] Fyta M G *et al*, *Multiscale coupling of molecular dynamics and hydrodynamics: application to DNA translocation through a nanopore*, 2006 *Mult. Mod. Simul.* **5** 1156